



HAL
open science

Bacteriophage-Templated Assembly of Magnetic Nanoparticles and Their Actuation Potential

Agata Olszewska-widdrat, Mathieu Bennet, Frank Mickoleit, Marc Widdrat, Christophe Tarabout, Victoria Reichel, Katja Arndt, Dirk Schüler, Damien Faivre

► **To cite this version:**

Agata Olszewska-widdrat, Mathieu Bennet, Frank Mickoleit, Marc Widdrat, Christophe Tarabout, et al.. Bacteriophage-Templated Assembly of Magnetic Nanoparticles and Their Actuation Potential. ChemNanoMat, 2021, 7 (8), pp.942-949. 10.1002/cnma.202100053 . hal-03296301

HAL Id: hal-03296301

<https://amu.hal.science/hal-03296301v1>

Submitted on 23 Jul 2021

HAL is a multi-disciplinary open access archive for the deposit and dissemination of scientific research documents, whether they are published or not. The documents may come from teaching and research institutions in France or abroad, or from public or private research centers.

L'archive ouverte pluridisciplinaire **HAL**, est destinée au dépôt et à la diffusion de documents scientifiques de niveau recherche, publiés ou non, émanant des établissements d'enseignement et de recherche français ou étrangers, des laboratoires publics ou privés.



Distributed under a Creative Commons Attribution 4.0 International License

Bacteriophage-Templated Assembly of Magnetic Nanoparticles and Their Actuation Potential

Agata Olszewska-Widdrat,^{*,[a]} Mathieu Bennet,^[b] Frank Mickoleit,^[c] Marc Widdrat,^[d] Christophe Tarabout,^[e] Victoria Reichel,^[f] Katja Arndt,^[g] Dirk Schüler,^[h] and Damien Faivre^{*,[i]}

Abstract: Magnetic chains are of fundamental and technological interest. However, 1D assemblies of magnetic nanoparticles are only metastable such that their controlled organization requires the use of templates. Bacteriophages are human-inoffensive viruses with a filamentous morphology that have been shown to exhibit great potential in materials research. Here, we thus utilized the M13 phage as a model for the formation of actuated magnetite nanoparticle

superstructures. First, we built a sperm-like ensemble by covalently attaching magnetic nanoparticles to the head of the phage. Second, chain-like assemblies are obtained based on the electrostatic interactions between positively-charged magnetite nanoparticles attached to the negatively-charged phage surface. The nanoparticles-phages assembly is steered by external magnetic fields. We anticipate such materials can find applications in nanotechnology or nanomedicine.

Introduction

The spontaneous arrangement of molecules into organized manners has evolved as a prospective approach towards the development of novel materials.^[1] The construction of such materials often needs the growth control, the stability and the arrangement of nanoparticles.^[2] Magnetic nanoparticles, especially iron oxides, have been extensively used in the recent years as a building block for such nanomaterials.^[3] Surface-functionalized iron oxide nanoparticles, due to their low cytotoxicity, can be used in magnetic resonance imaging,^[4,5] drug delivery or magnetic hyperthermia, or to improve gene

therapy methods.^[6,7] In general, iron oxide nanoparticles are difficult to organize due to their magnetic properties and their controlled assembly is challenging because nanoparticles at the end of chains will tend to attract each other, thereby forming ring structures.^[8,9] The assembly of iron oxide nanoparticles usually occurs on supporting template surfaces to form 1D chains,^[10,11] 2D superlattices^[12] and 3D superstructures.^[13,14] Linear polyelectrolytes in solution deliver a 1D scaffold for the adsorption of metal ions with opposite charges, whereas 2D and 3D structures are based on either liquid oil/water assembly or on the increase the particle area density and the number of layers formed by self-assembly on a substrate.^[15,16] Also as a

[a] Dr. A. Olszewska-Widdrat
Department of Bioengineering
Leibniz Institute for Agricultural Engineering and Bioeconomy
Max-Eyth-Alle 100, 14469, Potsdam (Germany)
E-mail: aolszewska-widdrat@atb-potsdam.de
agata.olszewska@mpikg.mpg.de

[b] Dr. M. Bennet
cellenion SASU 60 Avenue Rockefeller, Bioparc Laennec, 69008 Lyon (France)
E-mail: Mathieu.bennet@mpikg.mpg.de

[c] Dr. F. Mickoleit
Department of Microbiology
University of Bayreuth
Universitätsstraße 30, 95447 Bayreuth (Germany)
E-mail: Frank.Mickoleit@uni-bayreuth.de

[d] Dr. M. Widdrat
Faculty of Medicine
Health and Medical University of Potsdam
Olympischer Weg 1, 14471 Potsdam (Germany)
E-mail: marc.widdrat@mpikg.mpg.de


[e] Dr. C. Tarabout
Department of Biomaterials
Max Planck Institute of Colloids and Interfaces
Am Mühlenberg 1
14476 Potsdam/Potsdam-Golm (Germany)
E-mail: christophe.tarabout@mpikg.mpg.de


[f] Dr. V. Reichel
Laboratoire Matière et Systèmes Complexes
UMR 7057 CNRS
Université 12 Diderot Paris 7, 75205 Paris Cedex 13 (France)
E-mail: victoria.reichel@mpikg.mpg.de


[g] Prof. Dr. K. Arndt
Department of Biochemistry and Biology
University of Potsdam
Karl-Liebknecht-Str. 24–25, 14476 Potsdam (Germany)
E-mail: katja.arndt@uni-potsdam.de

[h] Prof. Dr. D. Schüler
Department of Microbiology
University of Bayreuth
Universitätsstraße 30, 95447 Bayreuth (Germany)
E-mail: Dirk.Schueler@uni-bayreuth.de

[i] Dr. D. Faivre
Aix-Marseille Université
CEA, CNRS, BIAM
13108 Saint Paul lez Durance (France)
E-mail: Damien.FAIVRE@cea.fr
damien.faivre@mpikg.mpg.de

 Supporting information for this article is available on the WWW under <https://doi.org/10.1002/cnma.202100053>

 This manuscript is part of a special collection: "Beyond Active Colloids: From Functional Materials to Microscale Robotics".

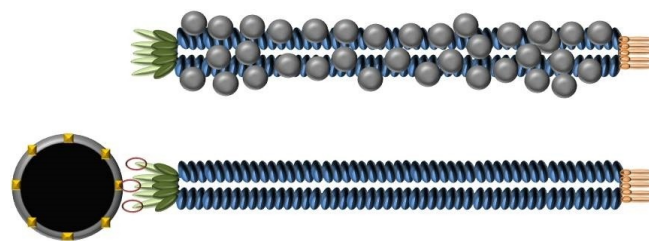
 © 2021 The Authors. ChemNanoMat published by Wiley-VCH GmbH. This is an open access article under the terms of the Creative Commons Attribution License, which permits use, distribution and reproduction in any medium, provided the original work is properly cited.

template, self-assembled block-copolymer structures, such as thin films, enable for a controlled assembly of magnetic nanoparticles.^[17,18] Bacteriophages (also called filamentous phages) comprise a potential substrate for the nanoparticle assembly. They constitute a large family of bacterial viruses that are being produced and secreted from infected bacteria without cell lysis. Original applications of bacteriophages were dedicated to molecular biology techniques. Phages were for example used as cloning vectors for sequencing and *in vitro* oligonucleotide-directed mutagenesis.^[19] Beside these applications, plasmids based on phages and called phagemids have been developed.^[20] More recently, phages have been used in medicine.^[21] Filamentous phages have been applied in a range of fields aside biology including biosensor production^[22–24] and supramolecular structure formation.^[25] Bacteriophages have furthermore been utilized in the development of new materials through either chemical^[26] or genetic approaches^[20] in order to display specific binding sites for tumor cells or surfaces.^[27,28] Specifically, the filamentous bacteriophage M13 is a long, flexible filament, approximately 6 nm in diameter and 1 μm in length.^[29] The single-stranded DNA genome is encapsulated in a tube made of helically arrayed major coat protein (P8). The tube is closed at each end by four proteins; P7, P9 on one end and P3, P6 on the other one.^[19] The P8 protein is the most abundant protein of the filamentous phage, representing 87% of its total mass and covering 99% of its total surface.^[30] Alternatively, the P3 protein is the most widely used system to display foreign peptides or proteins on the phage surface (phage display technology).^[31] This technique can be used to incorporate molecules capable of nanoparticle binding.^[30] All virion proteins have been used as a platform for display, but most commonly the minor P3 and the major P8 protein. Moreover, examples of the display of two or more proteins have been reported.^[32] The group of A. Belcher has exemplarily isolated peptides that can nucleate and/or assemble nanocrystals with varying properties, such as paramagnetic^[33] or semiconductor materials.^[34] But none of the above studies mentioned phages together with magnetite nanoparticles and their actuation by a magnetic field. Therefore, this work does not only show another approach related to the assembly of both phages and iron oxide nanoparticles but additionally provide a first step towards their actuation in external magnetic fields. Here, we focused on two types of nanoparticle assemblies: Sperm-like structures with a magnetic particle head covalently attached bacteriophage filament and chain of iron oxide nanoparticles attached to the phage tail via electrostatic interactions (see Scheme 1). Both of these constructs were further activated via an external magnetic field to show their potential as a device.

Results and Discussion

Formation of sperm-like assemblies

The sperm-like assemblies are expected to form from a single particle attached to a genetically modified P3 protein Figure 1. To achieve such a construction, we first fused mCherry to the C-



Scheme 1. A scheme of a schematic design of two constructs. The first one shows the electrostatic interaction between the phage filament and the PEI NPs (grey points). The second one represents the phage displaying mCherry (red ellipse) onto P3 phage protein (light green) attached to an RBP-magnetosome. The size of filaments and nanoparticles is not proportional.

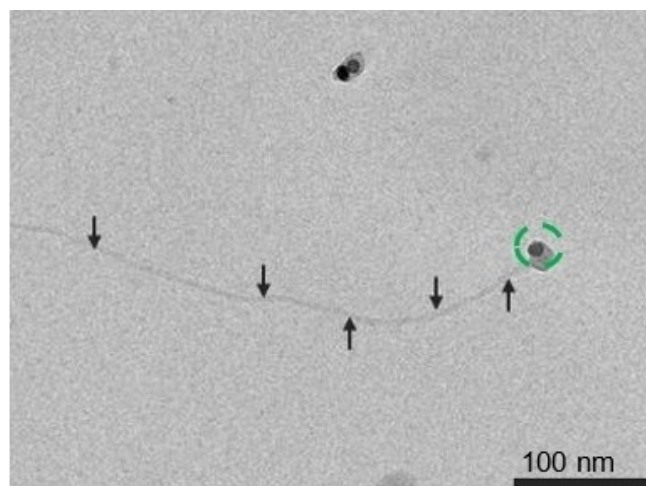


Figure 1. TEM image of the mCherry phage attached to the RBP-magnetosome.

terminal domain of the gene III protein of the phage following an established protocol.^[35] MamC-RBP magnetosomes were subsequently bound to mCherry phages. Magnetosomes are magnetic nanoparticles surrounded by the membrane and produced by magnetotactic bacteria.^[36] We choose MamC as membrane anchor for the red fluorescent protein binding nanobody (RBP) as this construct was already available^[37] such that the materials could be constructed by isolating magnetosomes from the available genetically modified strain.^[37] A similar approach was recently reported for the attachment of magnetosomes to particles of the tobacco mosaic virus.^[38] An exemplary mCherry phage binding to a single RBP-magnetosome is shown below (Figure 1). A magnetic head is surrounded by the green, dashed circle, whereas the tail is indicated by black arrows.

Nanoassemblies of RBP-magnetosomes and mCherry phages were investigated using fluorescence microscopy, which would constitute an alternative method to track the swimmers. It was possible to additionally stain the tail of the phages in order to detect at two fluorescence intensities. Fluorescent images recorded are shown in Figure 2. In Figure 2 a mCherry phage cluster can be observed, whereas in Figure 2b phages can be seen in green due to green fluorophore staining.

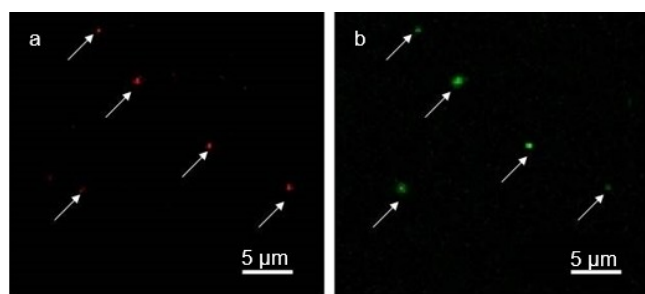


Figure 2. Fluorescence images of the mCherry phages. Fluorescence intensity images were recorded at a confocal microscope with the excitation wavelength at 561 nm and emission wavelength between 570 nm and 640 nm, corresponding to the fluorescence emission of the mCherry protein. Image (a) shows the mCherry phages. Image (b) shows mCherry phages stained with the green fluorophore.

The assembly of the mCherry phages and the RBP-magnetosomes makes studying the magnetic actuation of this hybrid material very promising. It is possible to use these nanostructures as swimmers, by actuating them with the magnetic fields. The assembly of the mCherry phages mixed with the RBP-magnetosomes was actuated in the magnetic field of 1 mT, at the frequency of 20 Hz. When the magnetic field was switched off, the elongated structure collapsed (Figure S1).

Individual components used as a basis for the chain – like assembly

Four types of nanoparticles were envisioned in the toolkit of the chain – like assembly. The list encompasses magnetosomes isolated from *M. magneticum* AMB-1 strain, magnetite nanoparticles synthesized without any additives,^[39] magnetite nanoparticles synthesized in the presence of poly-L-arginine^[40] and magnetite nanoparticles coated with the positively-charged polyethylenimine,^[41] (Figure 3). The nanoparticles were selected by their surface properties. Isolated magnetosomes tended to aggregate, mostly because of the magnetic interactions between single particles, but also due to residues of cellular compounds (such as proteins) that were left after the purification process and ‘glue’ nanoparticles together. Magnetite nanoparticles aggregated due to their magnetic attraction as well as the lack of organic (lipidic) membrane that ensure some steric hindrance (Figure 3b). Magnetite nanoparticles synthesized in the presence of poly-L-arginine (PolyR, Figure 3c) tended to form chains. Finally, PEI NPs shown in Figure 3d, appeared to be the best candidate to fulfil the requirements necessary for the deposition of nanoparticles on the phage filament. They were well-dispersed and did not aggregate in comparison with previously described nanoparticles, neither form chains. In Figure 3e, phage filaments stained with uranyl acetate are shown.

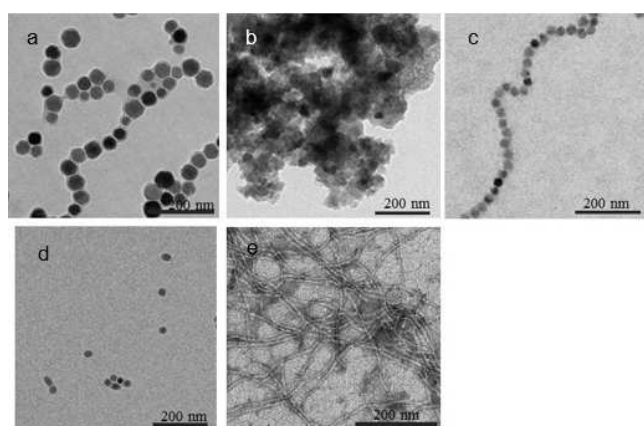


Figure 3. Transmission electron microscopy images of magnetosomes isolated from *M. magneticum* AMB-1 strain (a), magnetite nanoparticles synthesized without any additives (b), magnetite nanoparticles synthesized in the presence of poly-L-arginine (c), PEI NPs (d), WT phage filaments (e).

Electrostatic characterization of magnetite nanoparticles and phages

Zeta potential measurements were carried out on both the WT phages and the PEI NPs solution. For that purpose, phages and PEI NPs were suspended in a borate buffer. The zeta potential measurements showed that for all tested conditions ($5 < \text{pH} < 10$), the charge of the PEI NPs was positive (Figure 4, red circles). The zeta potential of PEI NPs was measured in the milli-Q water as well. In this case, the charge increased to 45 mV (Figure 4, dark blue arrow). At neutral pH, viral phage particles are mainly deprotonated and therefore have an overall negative charge. The zeta potential decreased to -39 mV when phage particles were dissolved in milli-Q water (Figure 4, purple arrow).

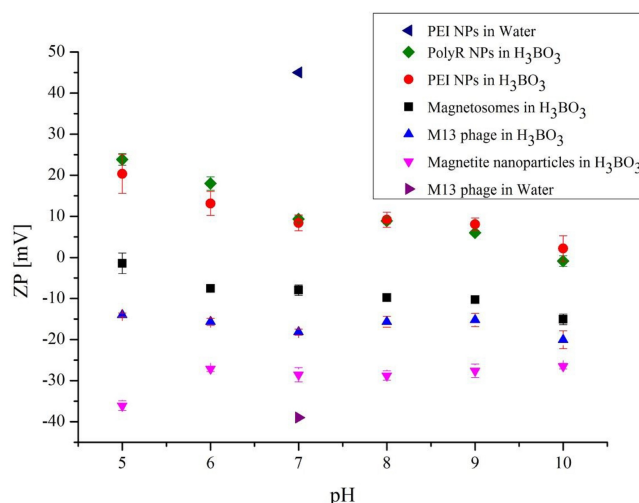


Figure 4. Zeta potential as a function of pH for PolyR nanoparticles (green diamonds), PEI NPs (red circles), WT magnetosomes (black squares), phage filaments (blue triangles), and magnetite nanoparticles (purple twisted triangles), dispersed in a borate buffer. PEI nanoparticles (blue arrow) and phage filaments (purple arrow) were additionally dispersed in milli-Q water.

Zeta potential measurements were carried out with all presented nanoparticles, starting from magnetite nanoparticles synthesized without any additives, WT magnetosomes isolated from *M. magneticum*, PolyR nanoparticles, and WT phage filaments.

Assembly of PEI NPs on the phage filament

One of the main characteristics of the M13 phage is its resistance to a wide range of pH and temperatures. Its N-terminus, which is exposed to the medium, contains negatively-charged amino acid residues. This region offers a number of functional groups that can be exploited for electrostatic interactions, for example with inorganic nanoparticles. The mixture of phages and nanoparticles was adsorbed on a silicone oxide substrate and imaged using TEM and AFM. The multi-valent assembly of PEI NPs on a single phage filament is shown in Figure 5a. Since the diameter of both particles (30 nm) and phages (6 nm) is known, it was possible to fit the height profiles with the appropriated parameters. PEI NPs, when adsorbed on the silicon oxide surface in the absence of any phage, exhibit high density aggregates without any defined pattern (see Figure S2 in SI). PEI NPs bind to the phage filament forming a chain-like organized structure, possibly due to electrostatic interactions between positively-charged PEI NPs and negatively-charged phage filaments (Figure 5b). In order to confirm that the particles are attached to the phage filament, the height profiles of PEI NPs and phage filaments were conducted (see

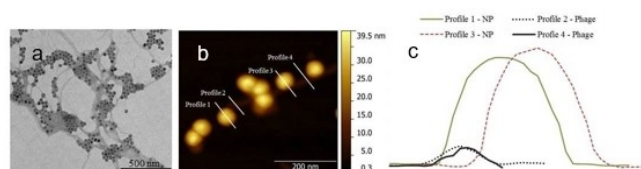


Figure 5. Assembly of PEI NPs attached to the phage filaments (a). Nanoparticles and phages were mixed in the ratio 2 : 1 and incubated 5 min in water. The mixture was placed onto the copper grid and stained with 2% uranyl acetate. Atomic force microscopy image of PEI NPs attached to the M13 phage (b); height profiles of M13 phage and PEI NPs attached to the phage filament (c).

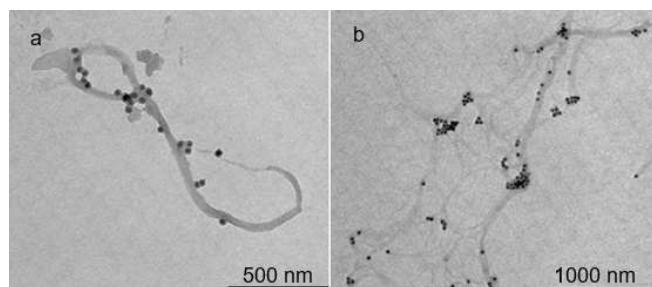


Figure 6. Transmission electron microscopy images of PEI NPs attached to phage filaments collected at the top of the vial, after 10 h of the magnetic actuation.

Figure 5c). Among all tested particles, only PEI NPs could be used for further magnetic actuation experiments.

Magnetic actuation of phage-nanoparticles assemblies

Phage-nanoparticles assemblies collected on the top of the capillary after 12 h are shown in TEM images, in Figure 6. Assemblies collected at the top of the vial showed different sizes and amorphous structures. Random shapes and unspecific distribution of nanoparticles onto phage filaments could be compared with the speed of collected structures constructed and measured by Vach et al,^[42,43] but so far no real data can be provided regarding phage-nanoparticles assembly.

Additional fluorescent staining of phage filaments was necessary in order to track the phage – nanoparticle assembly. Structures being tracked are shown in the Figure 7 and in the video in SI.

A mixture of labeled phage filaments and PEI NPs was actuated by a magnetic field of 1.4 mT, rotating at 30 Hz, what can be observed as a set of images (Figure 7). The red circle indicates the direction of the magnetic rotation. Red arrows are here to give the reader better ability to track the assembly.

Conclusion

In this study, two types of magnetic hybrid structures based on magnetite nanoparticles and M13 phages were investigated: sperm-like and chain-like assemblies. The first system, the sperm-like structure, was created by specific binding between the P3 protein of the phage filament, functionalized with the mCherry protein, and RBP magnetosomes, isolated from genetically modified *M. gryphiswaldense* MSR-1 strain. The second system, the chain-like structure, consisted of wild type phage filaments to which PEI magnetite nanoparticles were attached. The electrostatic interaction between the highly negative P8 protein of the phage and the positively-charged polyethylenimine shell of the magnetic nanoparticles enabled the attachment of the nanoparticles along the filament. These structures were actuated by external magnetic fields, exemplifying the possibility of their actuation potential for biotechnological applications.^[44] The magnetic control of the sperm – like swimmer was difficult due to its size. Higher yields of phages displaying mCherry protein would improve the visualization

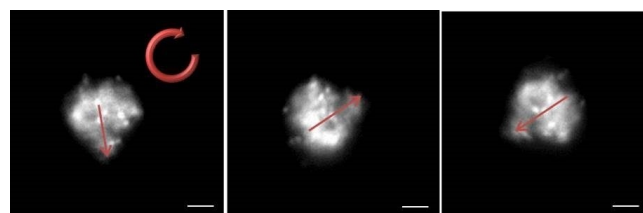


Figure 7. Fluorescence images of labeled phage filaments actuated in the magnetic field due to PEI NPs binding to their surface. Assembly is actuated by a magnetic field of 1.4 mT rotating at 30 Hz. Scale bar: 5 μ m.

techniques and enable phage-nanoparticle tracking. The improvement of micro-swimmer by modeling, for instance, the stiffness of the tail and the movement of magnetic filament, as studied by Roper et al. would have a potential.^[45] MamC-RBP - phage assembly comprises a new model to study with a flexible chain and the magnetic head. But not only is the motion important when designing such structures. It is possible to use other coat proteins in order to display peptides. For example, Hagen et al. successfully studied virus-directed enzyme prodrug therapy.^[46] Similar structures have been already investigated using other types of viruses^[38] On the other hand similar objects have been designed, so called nanobundles that have been fabricated using external magnetic field,^[47] but no external controlled actuation was reported. The movement of such hybrid materials is essential for the development of micro-swimmers and micro-robots in the medical field.^[48] Therefore, a fabrication of organized nanostructures leads to many approaches using different biotemplates, including proteins,^[49] viruses^[50,51] or filamentous bacteriophage.^[52,53] The transition to sub-micrometer dimensions creates challenges associated with fabrication and control of autonomous systems. Biological mobile nanoscale systems use similar operation modes as their engineered analogues and viruses are perhaps the most commonly occurring untethered mobile biological nanosystems.^[54] The development of small-scale robotics gives such devices a big chance to rise. Phage - based nanomedicine is an increasingly fast-growing field,^[55] where diagnostic of diseases via phage-nanoparticles assembly becomes a reality. By genetically modifying phages to bind to a specific target, bottlenecks and limitations in current approaches might be overcome. The latter include cancer treatment as well the increasing resistances against antibiotics. However, despite advanced techniques, the approval from the US Food and Drug Administration is obligatory in order to support, regulate and enhance the evaluations of the physico-chemical characterization of nanomaterials incorporated into medical devices.

Experimental Section

RBP magnetosome isolation

Magnetosomes were isolated from *M. gryphiswaldense* MSR-1 strain. The cultures were grown as previously described in modified flask standard medium (FSM)^[27] and cultivated up to a final volume of 10 L. After harvesting the cells by centrifugation, magnetosomes were isolated using a protocol slightly modified from Lang and Schüler.^[56] Briefly, the pellet of *M. gryphiswaldense* cells was washed three times by 15 min centrifugation at 9,000 rpm (14,300×g) and at 4 °C using a washing buffer (WB) (10 mM Hepes, 5 mM EDTA, pH 7.4; 30 mL for each washing step). The cells were subsequently resuspended in 10 mL resuspension buffer (RB) (50 mM Hepes, 1 mM EDTA, pH 7.4) and disrupted by 5 passages through a microfluidizer system (M-110L, Microfluidics Corp., Westwood, MA, USA), applying a pressure of 1.2×10^8 Pa. The resulting crude extract was passed through a MACS magnetic separation column (5 mL; Miltenyi Biotec, Bergisch Gladbach, Germany) to isolate the magnetosomes. Prior to loading the extract onto the column, the latter was equilibrated with extraction buffer (EB) (10 mM Hepes, 1 mM EDTA, pH 7.4). When subjecting the extract to the column,

the magnetosomes were retained due to the applied magnetic field. The particle-loaded column was firstly washed with ten column volumes of EB, secondly with ten column volumes of high salt buffer (10 mM Hepes, 1 mM EDTA, 200 mM NaCl), and again with ten column volumes of EB. Finally, the magnetic field was removed and the magnetosomes were eluted by adding milli-Q water to the column. As a further cleaning step, the magnetosome-containing suspension was subsequently ultracentrifuged through a 15 mL sucrose cushion (60% (w/v) sucrose in EB) at 200,000×g for 2 h at 4 °C, and the resulting pellet was resuspended in 5 mL EP.

WT magnetosome isolation

Magnetosomes were isolated from *M. magneticum* AMB-1 strain. AMB-1 cells were grown in a 16 L bioreactor. After harvesting the bioreactor and centrifuging the cells, the pellet of *M. magneticum* was washed three times with 30 mL washing buffer (10 mM Hepes, 5 mM EDTA, pH 7.4) by 15 min centrifugation at 9,000 rpm (14,300×g) and at 4 °C. 10 mL resuspension buffer (RB) (50 mM Hepes, 1 mM EDTA, pH 7.4) and 100 µL lysozyme [50 mg mL⁻¹] was added to the pellet and incubated for 30 min at 37 °C. Afterwards 5 mL of RB and 15 µL PMSF [100 mM] was added and the cell disruption (Modell TS; Constant cell Disruption System; UK) was performed at 2 kbar. To remove the cell debris, a centrifugation step (1,000 rpm, 5 min, 4 °C) was performed. The supernatant was poured into a glass beaker. Magnetic associated cell sorting (MAGS) was then used to remove all cell debris. The LS column (MACS Mitenyi Biotec; Germany) was placed into the MidiMACS Separator (MACS Mitenyi Biotec; Germany) and washed five times with sterile milli-Q water. The supernatant was added to the activated column and left to go through the column using the gravity force. The column with magnetosomes was firstly washed with five-fold of column volume of WB, secondly with the five-fold of column volume of high salt buffer (10 mM Hepes; 1 mM EDTA; 200 mM NaCl), and finally, with the fifth fold column volume of milli-Q water. For the elution step, the MidiMACS was removed and 2.5 mL EB was added to column and incubated for 15 min at RT to elute the magnetosomes. The fraction was flushed out and 2.5 mL milli-Q water was added. The elution procedure was repeated and the magnetosomes were collected in a glass beaker.

Polyarginine nanoparticles synthesis

Magnetite nanoparticles were synthesized in the presence of poly-L-arginine as described before.^[57]

Synthesis of magnetite nanoparticles without additives

The pure magnetite nanoparticles were synthesized as described before.^[58]

PEI nanoparticles

Positively charged iron oxide nanoparticles (PEI NPs), 30 nm in diameter, coated with amphiphilic polymer and polyethylenimine (PEI), were procured from Ocean NanoTech (San Diego, USA).

Genetically-modified mCherry phage

The mCherry phages were amplified according to a previously published procedure that was slightly modified.^[35] Briefly, 5 mL of 2xYT medium containing 25 µg mL⁻¹ chloramphenicol, 20 µg mL⁻¹ tetracycline and 1% glucose (2xYT/Cm/Tet/Glc) were inoculated with cells from a glycerol stock of *Escherichia coli* XL1-Blue

containing the respective phagemid. Cells were grown overnight at 37 °C on an orbital shaker (300 rpm). 60 mL of 2xYT/Cm/Tet were inoculated with the pre-culture to an OD₆₀₀ of 0.07 and grown at 37 °C with shaking (200 rpm). Cultures were infected with 10¹¹ particles of a helper phage VCS M13 at an OD₆₀₀ of 0.3 to 0.4. After 15 min incubation without shaking, g3p-fusion protein expression was initiated with 0.8 mM isopropyl β-thiogalactopyranoside (IPTG) and shaking was continued at 28 °C (if not stated otherwise). After 1 h, kanamycin was added to a final concentration of 70 μg mL⁻¹. After 5 h, the bacterial cells were removed by two successive centrifugation steps (5,000 × g, 15 min, 4 °C) and the upper 80% of the supernatant were taken and mixed with one-sixth volume of polyethylene glycol (PEG)/NaCl solution (20% PEG 8000, 2.5 M NaCl). After overnight incubation on ice, the sample was centrifuged (5,000 × g, 45 min, 4 °C) and the pellet was dissolved in 1 mL Tris-buffered saline (TBS) (25 mM Tris/HCl, 150 mM NaCl, pH 7.5). Impurities were removed by centrifugation (16,060 × g, 10 min, and 4 °C) and the phage particles were precipitated by mixing the supernatant with 200 ml PEG/NaCl solution and 1 h incubation on ice. The phage particles were again collected by centrifugation (16,060 × g, 10 min, 4 °C) and dissolved in TBS. After another centrifugation step (16,060 × g, 10 min, 4 °C), the upper 90% of the supernatant were taken and the phage content was determined by absorption measurement by the absorption measurement according to.^[59]

$$\text{Phage concentration (phages/ml)} = \frac{(A_{269} - A_{320}) \times 6 \times 10^{16}}{\text{phage genome in nt} \times \text{dilution factor}} \quad (1)$$

The wild type (WT) bacteriophage

The M13KE phages were purchased from New England Biolabs (Ipswich, Massachusetts, USA). The phages were grown and purified with standard biochemical protocols. Briefly, *E. coli* K12 ER2738 was used for the phage amplification. 20 mL of a medium was inoculated with 200 μL overnight *E. coli* culture and 1 μL phage suspension was added. The ER2738 cells were incubated at 37 °C under vigorous shaking (250 rpm) for 4.5 h. After cell removal by two centrifugation steps (4,500 × g, 10 min, and 4 °C), the top 16 mL supernatant were transferred to a new tube and mixed with 2.5 M NaCl/20% PEG-8000 (w/v) solution to concentrate the phage solution. After overnight precipitation at 4 °C, the phage pellet was collected by centrifugation at 12,000 × g, 15 min and resuspended in 1 mL milli-Q water. After a second precipitation step with 2.5 M NaCl/20% PEG - 8000 (w/v), the final phage pellet was collected and suspended in 100 μL milli-Q water. The phage content was determined by the absorption measurement according to.^[59] A large phage yield was necessary to perform the zeta potentials measurements. Therefore, the standard amplification protocol described above was scaled up to the final volume of 1 mL of the phage solution.

Zeta Potential determination

Dynamic Light Scattering of the M13 phages, the iron oxide nanoparticles and a mixture of M13 and PEI NPs was carried out with a Zetasizer ZEN ZS 3500 (Malvern Instruments, Malvern, UK). The nanoparticles of interest and the phage solution were poured into a clean cuvette designed for the zeta potential measurements. 1 mL solution was applied for each run. Three runs were performed at 25 °C and each run was measured 20 times and averaged.

The zeta potential (ZP) experiments were performed in order to determine the surface charges of all of the tested nanoparticles and of the M13 virus in order to optimize conditions allowing the electrostatic binding. The ZP measurements were carried out in water and in a borate buffer solution. The influence of the ionic strength has a strong effect on the behavior of the molecules, but even in milli-Q water, the structure remained stable for at least one week. ZP measurements were the determining factor in choosing the final type of nanoparticles used for the assembly onto the phage filaments.

Transmission electron microscopy (TEM)

The nanoparticles were selected based on their surface properties. The magnetosomes isolated from *M. magneticum* AMB-1 strain, RBP magnetosomes,^[37] PEI NPs as well as phages were characterized in terms of size and amount using transmission electron microscopy (TEM). 20 μL of the suspension was adsorbed to a carbon film Cu TEM grid for 10 min. Prior to TEM analyses, the samples were negatively stained with 2% uranyl acetate solution. The excess staining solution was wicked off. The imaging was performed with a Zeiss 912 Omega at 120 kV.

Topography measurements with atomic force microscopy (AFM)

Topography measurements of the phages and nanoparticles were carried out with a commercially available AFM (Bruker Dimension AFM, Bruker). The experiments were performed with a silicon cantilever (Olympus AC160). 10 μL of phages, particles solution and phages mixed with particles were spread on a fresh SiO₂ substrate and allowed to dry for the imaging at ambient conditions. The AFM images were analyzed with the open-source program Gwyddion. The images were leveled by flattening and adjusting the height to obtain the zero height in the plane level. The profiles were exported and analyzed using Excel.

Fluorescence imaging using fluorescence confocal microscopy

The fluorescence imaging experiments were performed on a commercial confocal microscope (SP 5, Leica). The laser beam was scanned over the sample using the confocal setup through the objective (60X, 1.2 NA, Wl, Leica). The laser scanning and intensity sets were measured by the LASAF (Leica) software. The mCherry - phage solution was centrifuged in order to collect the phage pellet and washed by TBS buffer. This step was performed three times and the pellet was finally resuspended in an aqueous solution containing 1% low-melt agarose (Sigma-Aldrich) at 30 °C. 30 μL of the suspension were placed between a microscope slide and a coverslip. The agarose formed a gel after cooling of the sample down to room temperature such that the phages immobilized while imaged.

Optical microscopy with magnetic setup

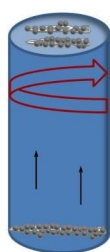
We used an in-house developed microscopic platform.^[60] Briefly, the sample to be analyzed was held in a non-magnetic sample holder, surrounded by a triaxial Helmholtz coil with controller (C-SpinCoil-XYZ, Micro Magnetics Inc.). The sample holder was positioned on a xyz motorized translation stage (PT3/M-Z8, Thorlabs and controlled by provided software (apt user application, Thorlabs)). In order to generate direct current (DC) magnetic fields 3D-axis Helmholtz coils were used. In both the alternating current

(AC) and the DC mode, the Earth's magnetic field could be cancelled. The magnetic field was applied with the help of Labview program. For imaging experiments, a high-speed camera (CR3000×2, Optronic) was used. The latter was controlled with the software developed by the supplier (Timebench, Optronic).

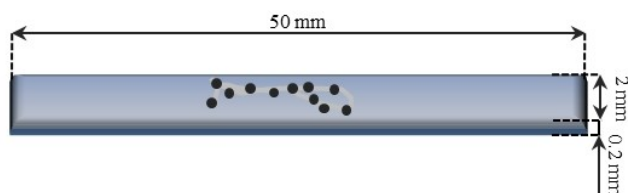
The phage filaments were incubated for one hour with succinimidyl ester (Alexa Fluor 488 NHS Ester, Life Technologies). After three washing steps, the phage solution was mixed with PEI NPs. This sample was finally investigated inside a glass capillary using the fluorescent microscope. Two excitation sources were combined using a dichroic mirror and the sample was illuminated through an objective (60X, NA 1.2, WI, Planapochromat, Nikon, GmbH). In order to enable the simultaneous use of the two cameras (high speed fluorescence) a beam splitter (Thorlabs) was located after the imaging lens. The fluorescent camera (Neo sCMOS, Andor) was controlled by using the Andor iQ software (Andor technology).

Selection of the swimming structures

40 μ L of a mixture of PEI NPs and M13 phage solution were deposited at the bottom of a glass vial containing 600 μ L milli-Q water, as shown in Scheme 2. The vial was placed in a rotating magnetic field in order to select and collect the swimming materials. Control experiments were performed: in the absence of a field to check whether the actuated propellers moved to the top of the surface due to other mechanism than magnetic actuation. Samples either with phages or with nanoparticles were placed between coils and magnetic field was applied. In the first case, phages were not detectable whereas nanoparticles were collected forming aggregates without specified shape. Faster phage – PEI NPs assemblies were collected at the top of the vial. A rotating magnetic field actuated the magnetic structures. Assemblies that were too large/too slow stayed at the bottom of the vial. In order to evaluate the potential use of phage-nanoparticle assemblies as magnetically actuated nanostructures, experiments were performed by actuating the assemblies with an external rotating magnetic field. The mixture of phage-nanoparticles was placed at the bottom of vials filled with 600 μ L of milli-Q water. The coils were producing



Scheme 2. Schematic that illustrates the swimmers selection process. The assembly moves to the top of the vial due to the forces that arise from the rotational and translator movement.



Scheme 3. Schematic of the capillary showing phage filaments and attached nanoparticles. The size of the capillary and the assembly is not proportional.

alternating and direct currents simultaneously. The magnetic field strength produced at the frequency of 20 Hz was 1.4 mT. Phage-nanoparticle assemblies, which were detectable after 10 h of the magnetic actuation, were collected from the top of the vial and analyzed via TEM.

The speed of magnetic chains was measured in another glass capillary (0.2×2×50 mm, Vitrotubes, Vitrocom). The mixture of phages and nanoparticles was filled into the capillary, shown in Scheme 3, which was subsequently placed in the microscope sample holder with the actuating magnetic field. The chains were directed to move to the upper surface of the capillary. Afterwards, the magnetic field was changed, so that the propeller was moving parallel to the capillary surface. The recorded videos were analyzed by manually searching for start and end positions, in between the structures were not disturbed by other assemblies. The measurement method was previously established.^[61]

Acknowledgements

The authors are grateful to Dr. Peter Vach for scientific discussions and Annegret Praast for laboratory work assistance. Open access funding enabled and organized by Projekt DEAL.

Conflict of Interest

The authors declare no conflict of interest.

Keywords: Magnetite · Nanoparticles · Assembly · Bacteriophage · Magnetosomes

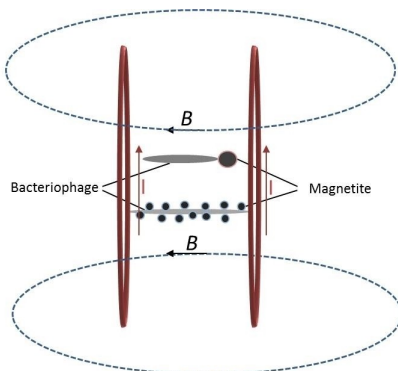
- [1] F. Versluis, J. H. van Esch, R. Eelkema, *Adv. Mater.* **2016**, *28*, 4576–4592.
- [2] E. Pouget, E. Grelet, *Langmuir* **2013**, *29*, 8010–8016.
- [3] F. Bachmann, K. Bente, A. Codutti, D. Faivre, *Phys. Rev. Appl.* **2019**, *11*, 1–12.
- [4] P. Yang, F. Wang, X. Luo, Y. Zhang, J. Guo, W. Shi, C. Wang, *ACS Appl. Mater. Interfaces* **2014**, *6*, 12581–12587.
- [5] S. Shukla, N. F. Steinmetz, *Wiley Interdiscip. Rev. Nanomed. Nanobiotechnol.* **2015**, *7*, 708–721.
- [6] K. Wu, D. Su, J. Liu, R. Saha, J. P. Wang, *Nanotechnology* **2019**, *30*, 502003.
- [7] M. G. Warner, J. E. Hutchison, *Nat. Mater.* **2003**, *2*, 272–7.
- [8] D. Faivre, M. Bennet, *Nature (News & Views)* **2016**, *535*, 235–236.
- [9] B. Kiani, D. Faivre, S. Klumpp, *PLoS One* **2018**, *13*, 1–17.
- [10] Z. Tang, N. A. Kotov, *Adv. Mater.* **2005**, *17*, 951–962.
- [11] L. Chen, B. Su, L. Jiang, *Chem. Soc. Rev.* **2019**, *48*, 8–21.
- [12] J. J. Benkoski, R. L. Jones, J. F. Douglas, A. Karim, *Langmuir* **2007**, *23*, 3530–7.
- [13] M. Giersig, M. Hilgendorff, *Eur. J. Inorg. Chem.* **2005**, 3571–3583.
- [14] G. Singh, H. Chan, A. Baskin, E. Gelman, N. Repnin, P. Kral, R. Klajn, *Science* **2014**, *345*, 1149–1153.
- [15] S. Nemeč, S. Kralj, *ACS Appl. Mater. Interfaces* **2021**, *13*, 1883–1894.
- [16] V. Du, N. Luciani, S. Richard, G. Mary, C. Gay, F. Mazuel, M. Reffay, P. Menasché, O. Agbulut, C. Wilhelm, *Nat. Commun.* **2017**, *8*, 1–12.
- [17] Y. Hu, L. He, Y. Yin, *Angew. Chem. Int. Ed.* **2011**, *50*, 3747–3750; *Angew. Chem.* **2011**, *123*, 3831–3834.
- [18] J. B. Chang, H. K. Choi, A. F. Hannon, A. Alexander-Katz, C. A. Ross, K. K. Berggren, *Nat. Commun.* **2014**, *5*, 1–17.
- [19] J. Rakonjac, *eLS* **2012**, DOI 10.1002/9780470015902.a0000777.
- [20] L. Chasteen, J. Ayriss, P. Pavlik, A. R. M. Bradbury, *Nucleic Acids Res.* **2006**, *34*, 1–11.
- [21] K. S. Sunderland, M. Yang, C. Mao, *Angew. Chem. Int. Ed.* **2017**, *56*, 1964–1992; *Angew. Chem.* **2017**, *129*, 1992–2022.

- [22] J.-W. Oh, W.-J. Chung, K. Heo, H.-E. Jin, B. Y. Lee, E. Wang, C. Zueger, W. Wong, J. Meyer, C. Kim, S.-Y. Lee, W.-G. Kim, M. Zemla, M. Auer, A. Hexemer, S.-W. Lee, *Nat. Commun.* **2014**, *5*, 1–8.
- [23] V. Liljeström, A. Ora, J. Hassinen, H. T. Rekola, N. Nonappa, M. Heilala, V. Hynninen, J. J. Joensuu, R. H. A. Ras, P. Törmä, O. Ikkala, M. A. Kostianen, *Nat. Commun.* **2017**, *8*, 1–10.
- [24] J. Y. Lee, H. Yi, W.-J. Kim, K. Kang, D. S. Yun, M. S. Strano, G. Ceder, A. M. Belcher, *Science* **2009**, *324*, 1051–1056.
- [25] N. Korkmaz, Y. J. Kim, C. H. Nam, *Macromol. Biosci.* **2013**, *13*, 376–387.
- [26] G. T. Hess, J. J. Cragnolini, M. W. Popp, M. A. Allen, S. K. Dougan, E. Spooner, H. L. Ploegh, A. M. Belcher, C. P. Guimaraes, *Bioconjugate Chem.* **2012**, *23*, 1478–1487.
- [27] J. M. Carrico, M. E. Farkas, Y. Zhou, S. C. Hsiao, J. D. Marks, H. Chokhawala, D. S. Clark, M. B. Francis, *ACS Nano* **2012**, *6*, 6675–6680.
- [28] J. Rakonjac, N. J. Bennett, J. Spagnuolo, D. Gagic, M. Russel, *Curr. Issues Mol. Biol.* **2011**, *13*, 51–76.
- [29] N. M. D. Courchesne, M. T. Klug, P. Y. Chen, S. E. Kooi, D. S. Yun, N. Hong, N. X. Fang, A. M. Belcher, P. T. Hammond, *Adv. Mater.* **2014**, *26*, 3398–3404.
- [30] J. Muzard, M. Platt, G. U. Lee, *Small* **2012**, *8*, 2403–2411.
- [31] G. P. Smith, V. A. Petrenko, *Chem. Rev.* **1997**, *97*, 391–410.
- [32] Y. Huang, C.-Y. Chiang, S. Kwan Lee, Y. Gao, E. L. Hu, J. De Yoreo, A. M. Belcher, *Nano Lett.* **2005**, *5*, 1429–1434.
- [33] C. Mao, D. J. Solis, B. D. Reiss, S. T. Kottmann, R. Y. Sweeney, A. Hayhurst, G. Georgiou, B. Iverson, A. M. Belcher, *Science* **2004**, *303*, 213–7.
- [34] S. R. Whaley, D. S. English, E. L. Hu, P. F. Barbara, A. M. Belcher, *Nature* **2000**, *405*, 665–8.
- [35] J. Speck, K. M. Arndt, K. M. Müller, K. M. Müller, *Protein Eng. Des. Sel.* **2011**, *24*, 473–484.
- [36] S. Klumpp, C. T. Lefèvre, M. Bennet, D. Faivre, *Phys. Rep.* **2019**, *789*, 1–54.
- [37] A. Pollithy, T. Romer, C. Lang, F. D. Müller, J. Helma, H. Leonhardt, U. Rothbauer, D. Schüler, *Appl. Environ. Microbiol.* **2011**, *77*, 6165–71.
- [38] F. Mickoleit, K. Altintoprak, N. L. Wenz, R. Richter, C. Wege, D. Schüler, *ACS Appl. Mater. Interfaces* **2018**, *10*, 37898–37910.
- [39] M. Widdrat, E. Schneck, V. Reichel, J. Baumgartner, L. Bertinetti, W. Habraken, K. Bente, P. Fratzl, D. Faivre, *J. Phys. Chem. Lett.* **2017**, *8*, 1132–1136.
- [40] V. Reichel, A. Kovács, M. Kumari, É. Bereczk-Tompa, E. Schneck, P. Diehle, M. Pósfai, A. M. Hirt, M. Duchamp, R. E. Dunin-Borkowski, D. Faivre, *Sci. Rep.* **2017**, *7*, 1–8.
- [41] L. Yang, X.-H. Peng, Y. A. Wang, X. Wang, Z. Cao, C. Ni, P. Karna, X. Zhang, W. C. Wood, X. Gao, S. Nie, H. Mao, *Clin. Cancer Res.* **2009**, *15*, 4722–4732.
- [42] P. J. Vach, P. Fratzl, S. Klumpp, D. Faivre, *Nano Lett.* **2015**, *15*, 7064–7070.
- [43] P. J. Vach, D. Faivre, *Sci. Rep.* **2015**, *5*, 1–6.
- [44] Q. A. Pankhurst, J. Connolly, S. K. Jones, J. Dobson, *J. Phys. D: Appl. Phys.* **2003**, *36*, 167–181.
- [45] M. Roper, R. Dreyfus, J. Baudry, M. Fermigier, J. Bibette, H. A. Stone, *Proc. Roy. Soc. A* **2008**, *464*, 877–904.
- [46] S. Hagen, T. Baumann, H. J. Wagner, V. Morath, B. Kaufmann, A. Fischer, S. Bergmann, P. Schindler, K. M. Arndt, K. M. Müller, *Sci. Rep.* **2014**, *4*, 3759.
- [47] S. Kralj, D. Makovec, *ACS Nano* **2015**, *9*, 9700–9707.
- [48] K. Bente, A. Codutti, F. Bachmann, D. Faivre, *Small* **2018**, *14*, 1–25.
- [49] F. Jehle, V. Valverde-Tercedor, C. Reichel, M. A. Carillo, M. Bennet, E. Günther, R. Wirth, F. Mickoleit, R. Zarivach, D. Schüler, K. G. Blank, D. Faivre, *Adv. Mater. Interfaces* **2017**, *4*, 1600285.
- [50] E. Dujardin, C. Peet, G. Stubbs, J. N. Culver, S. Mann, *Nano Lett.* **2003**, *3*, 413–417.
- [51] C. Koch, F. J. Eber, C. Azucena, A. Förste, S. Walheim, T. Schimmel, A. M. Bittner, H. Jeske, H. Gliemann, S. Eiben, F. C. Geiger, C. Wege, *Beilstein J. Nanotechnol.* **2016**, *7*, 613–629.
- [52] F. Li, Q. Wang, *Small* **2014**, *10*, 230–245.
- [53] W. C. Records, Y. Yoon, J. F. Ohmura, N. Chanut, A. M. Belcher, *Nano Energy* **2019**, *58*, 167–174.
- [54] I. Paprotny, S. Bergbreiter, *Springer*, **2013**, 1–15.
- [55] Y. I. Golovin, N. L. Klyachko, A. G. Majouga, M. Sokolsky, A. V. Kabanov, *J. Nanopart. Res.* **2017**, *19*, 1–47.
- [56] C. Lang, D. Schüler, *Appl. Environ. Microbiol.* **2008**, *74*, 4944–4953.
- [57] J. Baumgartner, M. Antonietta Carillo, K. M. Eckes, P. Werner, D. Faivre, *Langmuir* **2014**, *30*, 2129–2136.
- [58] J. Baumgartner, A. Dey, P. H. H. Bomans, C. Le Coadou, P. Fratzl, N. A. J. M. Sommerdijk, D. Faivre, *Nat. Mater.* **2013**, *12*, 310–4.
- [59] R. L. Wiseman, S. A. Berkowitz, A. Day, *J. Mol. Biol.* **1976**, *102*, 549–561.
- [60] M. Bennet, A. McCarthy, D. Fix, M. R. Edwards, F. Repp, P. Vach, J. W. C. Dunlop, M. Sitti, G. S. Buller, S. Klumpp, D. Faivre, *PLoS One* **2014**, *9*, 1–10.
- [61] P. J. Vach, N. Brun, M. Bennet, L. Bertinetti, M. Widdrat, J. Baumgartner, S. Klumpp, P. Fratzl, D. Faivre, *Nano Lett.* **2013**, *13*, 5373–8.
- [62] S. A. Alrumman, *Braz. J. Microbiol.* **2016**, *47*, 110–119.

Manuscript received: January 27, 2021
 Revised manuscript received: May 3, 2021
 Accepted manuscript online: May 17, 2021
 Version of record online: ■■■, ■■■■

FULL PAPER

This study introduces the formation of two types of nanoparticle assembly. First assembly, sperm-like, was based on covalent binding between the magnetic head and nonmagnetic tail, whereas the second one, chain-like assembly, was constructed using electrostatic interactions between the positively charged magnetic nanoparticles and the negatively charged filament. This study also shows first insights into magnetic actuation of such structures.



Dr. A. Olszewska-Widdrat, Dr. M. Bennet, Dr. F. Mickoleit, Dr. M. Widdrat, Dr. C. Tarabout, Dr. V. Reichel, Prof. Dr. K. Arndt, Prof. Dr. D. Schüler, Dr. D. Faivre**

1 – 9

Bacteriophage-Templated Assembly of Magnetic Nanoparticles and Their Actuation Potential

